Lab on a Chip

PAPER

View Article Online
View Journal | View Issue

Check for updates

Cite this: *Lab Chip*, 2021, **21**, 4791

A compact integrated microfluidic oxygenator with high gas exchange efficiency and compatibility for long-lasting endothelialization†

Julie Lachaux,[a] Gilgueng Hwang,[a] Nassim Arouche,[b] Sina Naserian,[b] Abdelmounaim Harouri,[a] Valeria Lotito,[a] Caterina Casari,[c] Thevy Lok,[d] Jean Baptiste Menager,[e] Justin Issard,[e] Julien Guihaire,[e] Cécile V. Denis,[c] Peter J. Lenting,[c] Abdul I. Barakat,[d] Georges Uzan,[b] Olaf Mercier[e] and Anne-Marie Haghiri-Gosnet*[a]

We have developed and tested a novel microfluidic device for blood oxygenation, which exhibits a large surface area of gas exchange and can support long-term sustainable endothelialization of blood microcapillaries, enhancing its hemocompatibility for clinical applications. The architecture of the parallel stacking of the trilayers is based on a central injection for blood and a lateral injection/output for gas which allows significant reduction in shear stress, promoting sustainable endothelialization since cells can be maintained viable for up to 2 weeks after initial seeding in the blood microchannel network. The circular design of curved blood capillaries allows covering a maximal surface area at 4 inch wafer scale, producing high oxygen uptake and carbon dioxide release in each single unit. Since the conventional bonding process based on oxygen plasma cannot be used for surface areas larger than several cm^2, a new "wet bonding" process based on soft microprinting has been developed and patented. Using this new protocol, each 4 inch trilayer unit can be sealed without a collapsed membrane even at reduced 15 μm thickness and can support a high blood flow rate. The height of the blood channels has been optimized to reduce pressure drop and enhance gas exchange at a high volumetric blood flow rate up to 15 ml min^{-1}. The simplicity of connecting different units in the stacked architecture is demonstrated for 3- or 5-unit stacked devices that exhibit remarkable performance with low primary volume, high oxygen uptake and carbon dioxide release and high flow rate of up to 80 ml min^{-1}.

Received 24th April 2021,
Accepted 7th July 2021

DOI: 10.1039/d1lc00356a

rsc.li/loc

Open Access Article. Published on 26 July 2021. Downloaded on 1/30/2026 5:49:22 PM.
This article is licensed under a Creative Commons Attribution 3.0 Unported Licence.

1. Introduction

The development of "artificial lungs" for clinical use was linked to the development of a heart–lung machine for heart surgery. Initially, the task was to design a reliable machine to oxygenate and decarboxylate blood. In the 1950s, oxygenators were based on direct contact of oxygen with blood.[1] Hemolysis with mechanical blood trauma was the main limiting factor for long-term use (only a few hours). In the 1980s, the benefit of adding a membrane system similar to a dialysis membrane was demonstrated, allowing long-term use (several weeks) and the advent of extracorporeal membrane oxygenation in intensive care units. However, these oxygenators offered high resistance to blood flow, had large surface areas that triggered inflammation and induced significant loss of plasma. As an alternative to ventilator support, extracorporeal membrane oxygenator (ECMO) therapy[2] has emerged with progress in long-term use ranging from a couple of weeks in venoarterial mode to several weeks in venovenous mode. However, ECMO therapy continues to require an intensive care unit, and hospital discharge on ECMO is not advisable. Latest-generation oxygenators still need to be changed within a couple of weeks because of clotting. One main reason is that perfusion within the oxygenators is not homogeneous, leading to low-flow (near stagnation) zones.

In this context, several groups have been investigating the implementation of microchannels in extra-corporeal exchange devices with the goal of considerably increasing the

[a] *Université Paris-Saclay, CNRS, Centre de Nanosciences et Nanotechnologies C2N, UMR9001, Palaiseau 91120, France. E-mail: anne-marie.haghiri@c2n.upsaclay.fr*
[b] *Université Paris-Saclay, INSERM, UMR-S-MD 1197, Hôpital Paul Brousse, Villejuif, France*
[c] *Université Paris-Saclay, INSERM, UMR S1176, Le Kremin-Bicêtre, France*
[d] *LadHyX, CNRS, Ecole polytechnique, Institut polytechnique de Paris, Palaiseau 91120, France*
[e] *Université Paris-Saclay, INSERM UMR_S 999 "Pulmonary Hypertension: Pathophysiology and Novel Therapies", Hôpital Marie Lannelongue, Le Plessis-Robinson, France*

† Electronic supplementary information (ESI) available. See DOI: 10.1039/d1lc00356a

Open Access Article. Published on 26 July 2021. Downloaded on 1/30/2026 5:49:22 PM.
This article is licensed under a Creative Commons Attribution 3.0 Unported Licence.

surface-to-volume ratio of the blood flow. The first proposed microfluidic oxygenators were based on a gas exchange trilayer structure where both air and blood microchannels exhibit dimensions comparable to lung capillaries.[3–6] While promising oxygen transfer rates were obtained, such systems were limited to blood flow rates in the range of a milliliter per minute. Thus, enhancing flow rate without reducing oxygenation performance remains a challenge for which scaling up appears as a pertinent solution.

The first proposed approach consists of connecting together in parallel several units to increase the total capacity in terms of blood volume.[3–11] The device proposed by Rieper *et al.*[11] was the first to attain blood flow rates of up to 50 ml min^{-1} for 10 stacked conventional trilayer units with an oxygen and carbon dioxide transfer of 3 ml O_2 per min and 3.6 ml CO_2 per min, respectively. Their fabrication process, which was amenable to industrialization, was also able to minimize the steric hindrance of the connectors. The gas exchange membrane thickness was 100 μm and the blood channels consisted of 1 mm-wide linear channels aligned in parallel. In 2019, Potkay's team[12] proposed an optimized design for one single-layer unit based on a closed-form mathematical model previously developed.[4] With a large exchange surface area of 0.31 m^2, this optimized single-layer device exhibits an oxygen uptake of 0.4 ml O_2 per min at a rated blood flow of 17 ml min^{-1} with a theoretical priming volume reduced to 0.40 ml and a capillary wall shear stress of 45 dyn cm^{-2}. Despite this progress, there is room for further miniaturization of channel and membrane geometries for the optimization of gas exchange efficiency and not only oxygen uptake but also carbon dioxide release. In addition, a biomimetic design warrants consideration for the optimization of the flow dynamics. Simplification of the fabrication/assembly process is another remaining challenge for further scaling up.

The second approach was dedicated to the enhancement of the exchange surface area either by using larger blood channels[13–15] or by exposing the two faces of the blood network to gas.[13–17] Dabaghi *et al.*[17] proposed a flexible device composed only of 1 mm-wide blood capillaries that are sandwiched between two membranes. The PDMS membranes that are mechanically reinforced by another polymer grid are in direct contact with ambient air, preventing the use of gas flow in confined structures. In addition, because of its high mechanical stability, this device can be folded or rolled into a compact shape to be inserted inside an oxygen bag. With a surface area for gas exchange of 0.01 m^2, this double-sided microfluidic blood oxygenator produces an oxygen and carbon dioxide transfer rate of 87.7 ml O_2 per min m^{-2} and 75.5 ml CO_2 per min m^{-2}, respectively, at a blood flow rate of 20 ml min^{-1}. Although promising for maintaining oxygen saturation at normal levels for preterm neonates, this approach is limited to low blood volume since parallel assembly would reduce the compactness of the device due to external connections.[18] A higher capacity can be achieved by parallel planar stacking. Also, oxygen uptake and carbon dioxide release can be maintained at a high level if the thickness of the membrane is significantly reduced. Based on PDMS membranes with a thickness in the range of 40–100 μm, all these approaches have a limited oxygen transfer rate at high flow. This is primarily due to the complexity of fabrication and the difficulty in sealing an ultra-thin membrane without compromising the mechanical stability of the trilayer structure of the oxygenator.

Further approaches to avoid mechanical blood stress and clots could be maintaining the shear rate within the microchannel network uniform and covering the inside of the microchannels with anticoagulant biomaterials and/or endothelial cells. Incorporating endothelial cells in such microchannel designs will produce a physiological nonthrombogenic and anti-inflammatory surface of blood microvessels, enhancing the long-term hemocompatibility of the microfluidic oxygenator. In their pioneering work, Gimbel *et al.*[19] showed that endothelial cells were not activated during the experiment, can maintain their anti-thrombotic phenotype and finally do not alter oxygen transfer in such biomimetic oxygenators.[19] More recently, Hellmann *et al.*[20] studied the hemocompatibility of endothelial cells seeded on peptide RGD-conjugated polydimethylsiloxane (RGD-PDMS) gas exchange membranes under dynamic conditions. Their work has demonstrated the ability to maintain a dynamic culture of endothelial cells under a flow rate of 1.2 ml min^{-1} corresponding to a wall shear stress of 2.9 dyn cm^{-2} for up to 21 days.

Minimizing the fluidic resistance of blood microchannels should also be considered to reduce the pressure drop. To become an alternative to the clinically used ECMO systems, microfluidic oxygenators should address all these challenges and should allow working at a much higher blood flow rate, namely a few liters per minute. Additionally, protecting the thin and vulnerable membranes by sandwiching them between blood and air microchannels would be a robust and fail-safe solution towards clinical applications. In this context, developing an in-plane stackable microfabrication process of trilayer sandwich structure able to perfectly integrate at the 4 inch scale an ultra-thin membrane ($t < 20$ μm) appears to be of great interest. In this study, a 15 μm-thick membrane will be used to obtain a total thickness of around 25 μm after cell endothelialization, which will promote gas exchange properties similar to those previously reported.[11,12,19] In this regard, a new design of both blood and air microfluidic channel networks needs to be considered. To mimic the blood vascular network, the geometric configuration of the microchannels should be a hierarchical structure, where vessels become progressively smaller in length and diameter to minimize the mechanical load.[21] The branching should follow Murray's law,[22] which predicts the relation between the diameter of the parent vessel and that of the two daughter branches. In addition, if the network consists of symmetric bifurcations, an important consequence of Murray's law is that the wall shear stress remains constant throughout the vascular system.[23]

 This journal is © The Royal Society of Chemistry 2021

Open Access Article. Published on 26 July 2021. Downloaded on 1/30/2026 5:49:22 PM.
This article is licensed under a Creative Commons Attribution 3.0 Unported Licence.

Compared to previous approaches, we describe here a new compact and biomimetic microfluidic oxygenator that integrates planar stacked 4 inch trilayer units with a very thin PDMS membrane (thickness = 15 μm) over a large surface that maximizes gas exchange. The innovative 4 inch architecture combines a centered blood injector that follows Murray's law with 5 successive injection branches, a large gas exchange surface area with 200 μm-wide curved blood microcapillaries crossing circular air/O_2 microchannels and a circular reservoir to collect fully oxygenated blood. First, we show that such an injector is compatible with cell endothelialization over 12 days. With vertical inlet/outlets for blood and lateral inlets/outlets for gas, this device can be stacked with limited volume loss for interconnections. Secondly, we demonstrate that such a single 4 inch trilayer unit with blood capillaries designed in agreement with Potkay's model and perfectly bonded to the 15 μm-thick membrane is able to sustain a high flow rate while maintaining remarkable gas exchange properties. The effect of the height of the blood capillaries on the gas exchange is studied and discussed based on theoretical calculations. Finally, this circular architecture is used to demonstrate that several 4 inch oxygenator units can easily be stacked with a unique central blood inlet and minimal external interconnections reducing the total priming volume. The proposed microfluidic oxygenator achieves a range of oxygenation flow rates similar to other state-of-the-art systems but with minimum stack numbers, which provides opportunities for further enhancing the blood flow rate. Moreover, a record carbon dioxide release efficiency is obtained. The proposed biomimetic design that allows inner channel endothelialization is also scalable in both the horizontal and the vertical dimensions.

2. Materials and methods

2.1 Microfluidic design and architecture

As schematically shown in Fig. 1c, each single unit of the micro-oxygenator exhibits the conventional trilayer structure with two networks of microchannels that are separated by a 15 μm-thick porous membrane to promote gas exchange.

To maximize the area covered by blood capillaries, we propose a circular geometry with curved capillaries distributed around the central blood inlet (see Fig. 1a with blood flowing in the white regions). The curvature was defined to increase microchannel density and to minimize the overall device footprint. With an optimal curvature, such a design promotes maximal coverage of the blood network on the 4 inch wafer. The blood inlet is central whereby a circular ring retrieves the blood at the exit of the network of curved capillaries. The centered injection branched tree structure with 5 levels of decreasing microchannel width guarantees a highly uniform flow distribution inside the 256 microcapillaries. The width of each circular tree branch has been chosen following Murray's law to obtain 200 μm for the smallest microcapillaries ($W = d_5 = 200$ μm − $N = 5$ in the tree structure, with $d_4 = 316$ μm, $d_3 = 453$ μm, $d_2 = 921$ μm and $d_1 = 1535$ μm). Such a tree structure allows a uniform distribution of the flow inside the capillaries as well as reduction of shear stress at each connection. It should be noted here that our inlet tree structure does not strictly follow the commonly known Murray's law established mainly for circular 3D channels. Using Murray's law to design artificial vascular microfluidic networks for our blood microfluidic channels requires consideration of the generalized form of Murray's law to account for our device's geometrical constraints. The generalized Murray's law can be

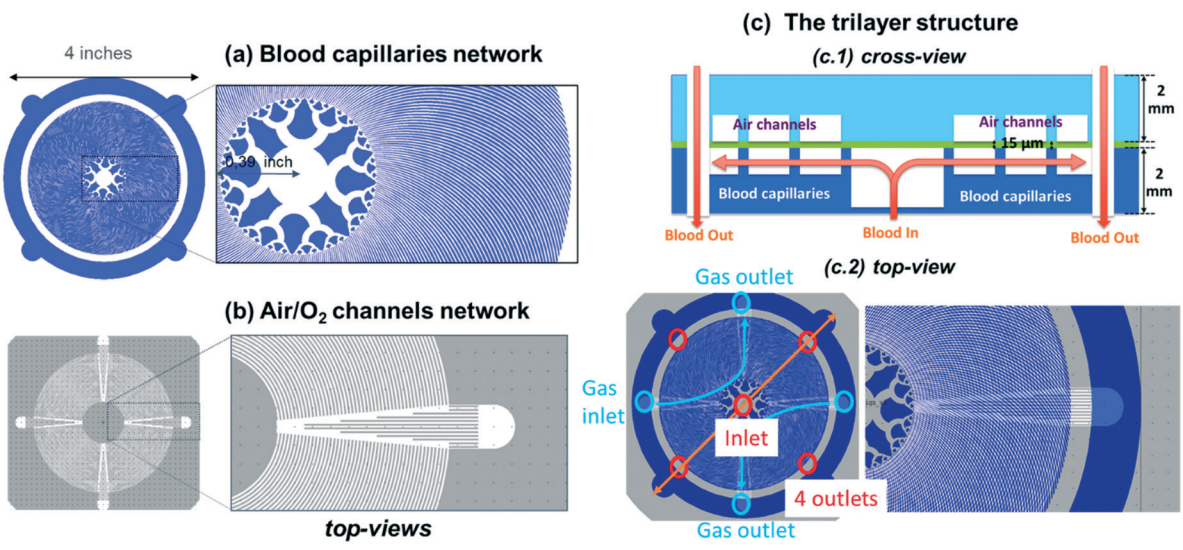

Fig. 1 Schematic top views of (a) the circular network of blood microcapillaries where blood flows in the white part and (b) the corresponding gas network, (c1) the schematic cross view of one single trilayer structure following the orange arrow in (c2) the top view of the superposed blood and air networks.

Open Access Article. Published on 26 July 2021. Downloaded on 1/30/2026 5:49:22 PM.
This article is licensed under a Creative Commons Attribution 3.0 Unported Licence.

applied to biomimetic designs for microfluidic systems composed of non-circular cross sections such as the constant-depth rectangular microfluidic manifolds that are often used in microfluidic systems.[23] The dimensions of the symmetric bifurcations from the inlet have been chosen to adapt the widths of the oxygen channels and the number of branches distributed to the 256 oxygen channels in a limited area. The dimensions of our bifurcation structure designs are in the range for reasonable shear stress[12] and also for fluidic resistance according to the generalized Murray's law.[23]

The cross-view of Fig. 1c1 explains how blood flows in the single trilayer structure. Four outlets are located on the diagonals of the circular ring for collecting blood (see red circles in Fig. 1c2). This geometry was also optimized for uniform flow distribution and integration of the 200 μm-wide curved microchannels. With an operating pressure drop below 80 mmHg, the microchannel height H was varied in the range of 85–105 μm to study how the pressure drop varies in the range of applicable flow rates, *i.e.* 0.5 to 15 ml min^{-1} for one single unit and 10 to 80 ml min^{-1} for 5 stacked units. The density of this blood capillary network also provides better mechanical strength than conventional structures. The design of the network of air (or oxygen) microchannels, which is presented in Fig. 1b, with four lateral planar inlets and outlets allows stacking several trilayers in a way suitable for injection of liquid and gas. The top view presented in Fig. 1c2 shows the alignment of the different levels inside the single trilayer unit. It allows optimizing the mechanical stability of entire capillaries while maintaining a large gaseous exchange surface. With a total surface area of opened membrane in the blood level of 0.0026 m^2, the effective gas exchange surface area after sealing the blood network with the air/O_2 network is reduced to 0.00107 m^2. Since all the patterns have been designed with L-edit software, this gas exchange surface has been calculated very easily using the Boolean function that allows subtracting the area of the blood network from that of the gas network in the circular region of capillaries (Fig. 1a and b). It is of importance to note that the radial curved design for the blood network and the circular design for the air/O_2 network allows enhancing capillary density and thus mechanical stability. This compactness of the blood network with a spacing between capillaries ranging from 50 μm to 200 μm from the central inlet of capillaries to the external ring outlet favors lateral gas transfer in addition to the normal vertical exchange through the thin membrane. Theoretical priming volume is also reduced to 0.27 ml compared to previous reported values, for example, 0.40 ml in the work of Thompson *et al.*[12]

To predict gas exchange efficiency, we used the mathematical model proposed by Potkay[4] that is fully adapted to describe gas exchange in microchannel artificial lungs. Potkay uses some assumptions to obtain a closed-form set of equations describing oxygen and carbon dioxide partial pressure (PO_2 and PCO_2), as well as oxygen saturation ($SatO_2$) at any flow rate and at any point in the device. This model helps in understanding the role of each parameter in gas exchange and thus designing capillary networks. The assumptions are as follows: (1) the blood capillaries are rectangular and separated from the air/O_2 channels by a gas exchange membrane; (2) oxygen and carbon dioxide partial pressures are constant in the air/O_2 channel; (3) diffusion is one-sided through the membrane; (4) blood is a homogenous fluid with an effective solubility and diffusivity for oxygen and carbon dioxide; (5) the blood side fluidic boundary layer for diffusion is equal to half the blood capillary height; (6) the partial pressure of gases in blood only varies along the length of the blood capillary and not along the blood capillary height or width; and, (7) the gas transport process is limited by diffusion of oxygen in blood plasma, not by diffusion into the red blood cell.

With these assumptions in place, the oxygen and carbon dioxide partial pressures at the outlet of the device are given by:

$$\mathrm{PO_{2,out}} = \mathrm{PO_{2,gas}} + \left(\mathrm{PO_{2,in}} - \mathrm{PO_{2,gas}}\right)\cdot \mathrm{e}^{-\frac{S_A}{Q\cdot S_{B,O_2}\cdot R_{O_2,tot}}}$$

$$\mathrm{PCO_{2,out}} = \mathrm{PCO_{2,gas}} + \left(\mathrm{PCO_{2,in}} - \mathrm{PCO_{2,gas}}\right)\cdot \mathrm{e}^{-\frac{S_A}{Q\cdot S_{B,CO_2}\cdot R_{CO_2,tot}}}$$

where $PO_{2,out}$ and $PCO_{2,out}$ are respectively the oxygen and carbon dioxide partial pressures at the outlet of the device; $PO_{2,in}$ and $PCO_{2,in}$ are respectively the oxygen and carbon dioxide partial pressures at the inlet of the device; $PO_{2,gas}$ and $PCO_{2,gas}$ are respectively the oxygen and carbon dioxide partial pressures in the oxygenation gas (air or O_2); S_A is the exchange surface area; Q is the blood volumetric flow rate; S_{B,O_2} and S_{B,CO_2} are respectively the effective solubility of oxygen and carbon dioxide in blood; and $R_{O_2,tot}$ and $R_{CO_2,tot}$ are respectively the total resistance to diffusion for oxygen and for carbon dioxide.

The total resistance for oxygen and carbon dioxide is written in this form:

$$R_{O_2,tot} = \frac{e_m}{P_{m,O_2}} + \frac{\frac{H}{2}}{S_{B,O_2}\cdot D_{B,O_2}}$$

$$R_{CO_2,tot} = \frac{e_m}{P_{m,CO_2}} + \frac{\frac{H}{2}}{S_{B,CO_2}\cdot D_{B,CO_2}}$$

where e_m is the membrane thickness; P_{m,O_2} and P_{m,CO_2} are respectively the permeabilities of the membrane (PDMS) to oxygen and carbon dioxide; H is the blood capillary height; and D_{B,O_2} and D_{B,CO_2} are respectively the effective diffusivities of oxygen and carbon dioxide in blood. S_{B,O_2} and S_{B,CO_2} are estimated to be 3.65×10^{-4} ml O_2 per ml blood per mmHg and 5.05×10^{-3} ml O_2 per ml blood per mmHg, respectively. D_{B,O_2} and D_{B,CO_2} are estimated to be 4.89×10^{-6} cm^2 s^{-1} and 3.05×10^{-6} cm^2 s^{-1}, respectively. Details on the methodology for the estimation of the effective solubility and diffusivity for

 This journal is © The Royal Society of Chemistry 2021

Open Access Article. Published on 26 July 2021. Downloaded on 1/30/2026 5:49:22 PM.
This article is licensed under a Creative Commons Attribution 3.0 Unported Licence.

oxygen and carbon dioxide in blood are presented in the ESI,† SI.1A and B. The oxygen–hemoglobin dissociation curve relates the partial pressure of oxygen in blood (PO_2) to the oxygen saturation ($SatO_2$) as described by the Hill equation:[24]

$$SatO_2 = \frac{(PO_2/P_{50})^n}{1 + (PO_2/P_{50})^n}$$

where P_{50} is the partial pressure of oxygen for a 50% saturation ($SatO_2$ = 0.5) and n is the Hill coefficient. For porcine blood under normal conditions (T = 37 °C and pH 7.4), P_{50} and n are estimated to be 35.7 mmHg and 2.94.[25]

Thanks to this mathematical model, the theoretical variation between the input and the output of the device for oxygen and carbon dioxide partial pressures (ΔPO_2 and ΔPCO_2) as well as oxygen saturation ($\Delta SatO_2$) were further used to estimate O_2 uptake and CO_2 release, and then O_2 and CO_2 exchange efficiencies (see the ESI† SI.1C for details).

2.2 Fabrication process and stacking

The whole device including the thin membrane, blood capillaries and air/O_2 microchannels is made of polydimethylsiloxane (PDMS) because of its high gas permeability and good hemocompatibility. In addition, the choice of the same material for all parts of the device facilitates the bonding process. To integrate the ultra-thin membrane between the two microchannel networks, a bonding protocol based on a very thin layer of uncured PDMS diluted in hexane was developed and patented.[26] The dilution of PDMS in hexane provides by spin coating a very thin layer used as a glue. This technique, based on soft micro-printing, allows efficient bonding even on surfaces as large as 4 inches.

The fabrication process is shown in Fig. 2. The negative templates corresponding respectively to the blood vascular network and to the gas network were fabricated with a conventional photolithography technique using SU-8 photoresist (SU-82050, Microchem). First, the PDMS mixture (RTV 615, Momentive Performance Material) with a volume ratio of 10 : 1 by weight (base and curing agent) was cast on the template of the gas network. The PDMS and the template were placed under a desiccator for 2 hours to degas the PDMS and then cured in an oven at 60 °C overnight (Fig. 2a). After curing, the PDMS gas network was peeled off from the template. A biopsy punch was used to remove the PDMS at the inlets and the outlets of the gas network (Fig. 2b).

The PDMS membrane was fabricated by spin-coating a layer of PDMS (volume ratio of 10 : 1) on a silicon wafer (Si wafer A) at a speed of 4000 rpm for 60 s and then cured in an oven at 60 °C for 4 hours. To reduce adhesion to PDMS, the blank silicon wafer (Si wafer A) was initially coated with Optool DSX (Daikin Industries, LTD). The thickness of the resulting membrane controlled by calibration of the spin coater was about 15 μm, as observed on cross sections using scanning electron microscopy (Fig. 2c and i).

For the bonding, a solution of PDMS (volume ratio of 10 : 1) diluted in hexane was prepared with a volume ratio of 1 : 4 by weight (10 g of PDMS and 40 g of hexane). The solution was placed in a mixer for 30 s to obtain a homogeneous mixture. This solution was used to obtain a 2 μm-thick wet

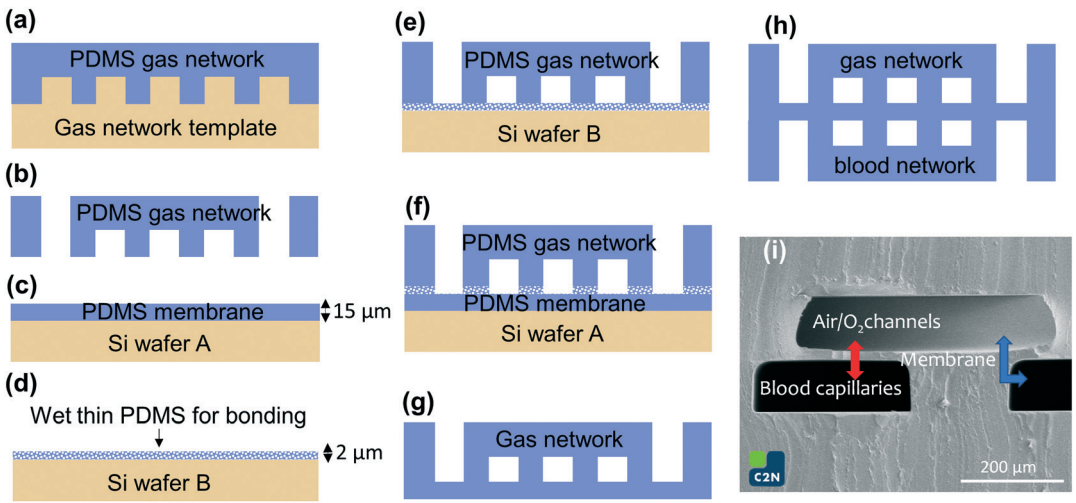

Fig. 2 Fabrication process of the 4 inch circular microfluidic oxygenator: (a) the gas network was obtained by casting PDMS on the SU-8 template and (b) after curing at 60 °C overnight and demolding, PDMS inside the two gas inlets and two gas outlets (Fig. 1c2) was removed with a biopsy punch, (c) the 15 μm-thin PDMS membrane was spin-coated on a silicon wafer and cured at 60 °C for 4 hours, (d) an ultra-thin (2 μm) PDMS/hexane layer was spin-coated on another silicon wafer (e) to wet the air/O_2 microchannel PDMS cover (f) that is placed on the 15 μm-thin membrane for 4 hours at 60 °C to ensure perfect sealing (g), steps (a and b) and (b) were repeated to prepare the PDMS blood network that was also sealed using the wet hexane/PDMS ultra-thin layer of steps (e) and (f) on the bilayer "air/O_2 PDMS cover/PDMS membrane" to obtain the perfectly sealed trilayer structure (h), (i) scanning electron micrograph showing a cross-view of the PDMS trilayer structure (arrows show where gas exchange occurs).

Open Access Article. Published on 26 July 2021. Downloaded on 1/30/2026 5:49:22 PM.
This article is licensed under a Creative Commons Attribution 3.0 Unported Licence.

layer of PDMS by spin-coating at a speed of 3000 rpm for 30 s on another silicon wafer (Si wafer B) (Fig. 2d). While the thin PDMS/hexane solution was still wet, the PDMS gas network was stamped in the wet PDMS/hexane thin layer and then immediately placed in contact with the PDMS membrane already fabricated on the Si wafer A (Fig. 2e and f). The whole bilayer was placed in an oven at 60 °C for 4 hours to evaporate hexane and cure the thin layer of PDMS between the membrane and the gas network, forming a very strong bonding. The PDMS bilayer was then peeled off from the wafer (Fig. 2g).

To obtain the blood vascular network in PDMS, steps (a) and (b) were repeated on the corresponding template. The blood vascular network was then stamped in a new solution of wet PDMS/hexane and then immediately put in contact with the previous PDMS bilayer made of membrane and gas network. The trilayer structure was placed in an oven at 60 °C for 4 hours to evaporate hexane and cure the thin wet layer of PDMS (Fig. 2h). A cross section of the trilayer structure visualized by scanning electron microscopy is shown in Fig. 2i allowing precise determination of the membrane thickness to be about $t = 15 \pm 1$ μm. The microchannels are geometrically well defined thanks to the quality of the photolithography process specifically developed to obtain high vertical structures in the SU-8 photoresist.[27] To test the bonding of the 4 inch devices and the mechanical stability of the trilayer structure, a burst pressure experiment was performed. No failure or leakage was observed below 600 mmHg.

Parallel stacking of multiple trilayer structures is very easy due to the centered architecture of this circular device. The parallel configuration allows significant expansion of the gas exchange capacity and the blood flow rate without increasing the pressure drop or the shear stress. Stacking of several single units was performed using the same bonding process, based on soft-microprinting, with a thin layer of uncured PDMS/hexane. The process was repeated until three (or five) layers were stacked together. As a reminder, blood capillaries and air/O_2 microchannels were designed in such a way that their crossing reinforces the mechanical stability of the stacked device. Finally, tubes with an interior diameter of 2.4 mm were positioned at the designed location of blood inlets and outlets on the bottom of the device for fluid circulation (NaCl or blood) and at the location of gas inlets on the top of the device for gas circulation (air or O_2). Note that there is no tubing on gas outlets because we do not need to recover the gas; it simply dissipates into the ambient air after circulating in the device.

2.3 Experimental set-up for gas exchange

A specific microfluidic experimental bench has been set up at Marie-Lannelongue Hospital to determine the gas exchange efficiency of the device using venous swine blood. To limit the number of animals used, we collect blood at the end of the procedure on animals already included in other protocols. The blood sampling procedure has been standardized as follows: after premedication and anesthesia of the animal (propofol IV (3 mg kg^{-1}, PROPOVET® 10 mg ml^{-1}, 20 ml ampoule)/cisatracurium (0.3 mg kg^{-1} NIMBEX®, 2 mg ml^{-1})/sufentanil IV (10 μg kg^{-1} h^{-1})), an endotracheal tube was placed for mechanical ventilation using a humidified gas mixture (heated to 38 °C) with FiO_2 (fraction of inspired oxygen) of 0.3 delivered at 8 L min^{-1}. The FiO_2 was then gradually decreased until the oxygen saturation dropped to 65%. Once the blood saturation had reached 65%, 500 ml of blood was collected in a bag through a 7 French sheath placed in the innominate venous trunk. At the end of the sampling procedure, the animal was euthanized by injection of sodium pentobarbital (veterinary use, 150 mg kg^{-1} IV). Heparin (5000 UI per liter) was then added into the collected blood. The blood bag was left at room temperature under agitation to prevent cell sedimentation.

The experimental set-up to characterize the gas exchange performance of the device is presented in Fig. 3a and b. Prior to circulating venous blood, saline solution (sodium chloride 0.9% B. Braun, solution for infusion) was used to flush and remove air from microfluidic capillaries. Subsequently, swine venous blood was pumped through the capillaries by a syringe pump (PHD 2000 Harvard Apparatus), while gas (air or O_2) was pushed through its network using a thermal mass flow meter (El-Flow, Bronkhorst) connected to an anesthesia respirator (Clarys 2000, Taema). The devices were tested by varying the blood flow rate with either pure O_2 or room air. The blood was systematically sampled at both input and output of the device for each condition (Fig. 3b). Analysis of blood, including oxygen partial pressure $P(O_2)$, carbon dioxide partial pressure $P(CO_2)$, oxygen saturation $Sat(O_2)$, pH, hematocrit (Hct) and total hemoglobin concentration [Hb], was carried out using an ABL800 FLEX radiometer. In addition, to measure the pressure drop during the experiment, a pressure transducer (TruWave from Edwards Lifesciences) connected to a Patient Monitor (90369, SpaceLabs Medical) was introduced at the entrance of the blood input capillaries. An image of a single-unit trilayer oxygenator under blood flow during the experiment is shown in Fig. 3c. Two videos recorded during the experiments with 3- and 5-stacked devices are also provided in the ESI† (see SI.4).

2.4 Method for endothelialization

Human samples were used in compliance with the Declaration of Helsinki. Cord blood (CB) samples from healthy full-term newborns were obtained from the CB Bank of St Louis Hospital (Paris, France), authorized by the French Regulatory Authority (no. PPC51). This activity was declared to and authorized by the French Ministry of Research under number AC-2008-376, and to the French Organization for standardization under number 201/51848.1. Mononuclear cells (MNCs), obtained by density gradient centrifugation, were seeded onto rat-tail collagen type I (CORNING) coated

 This journal is © The Royal Society of Chemistry 2021

Open Access Article. Published on 26 July 2021. Downloaded on 1/30/2026 5:49:22 PM.
This article is licensed under a Creative Commons Attribution 3.0 Unported Licence.

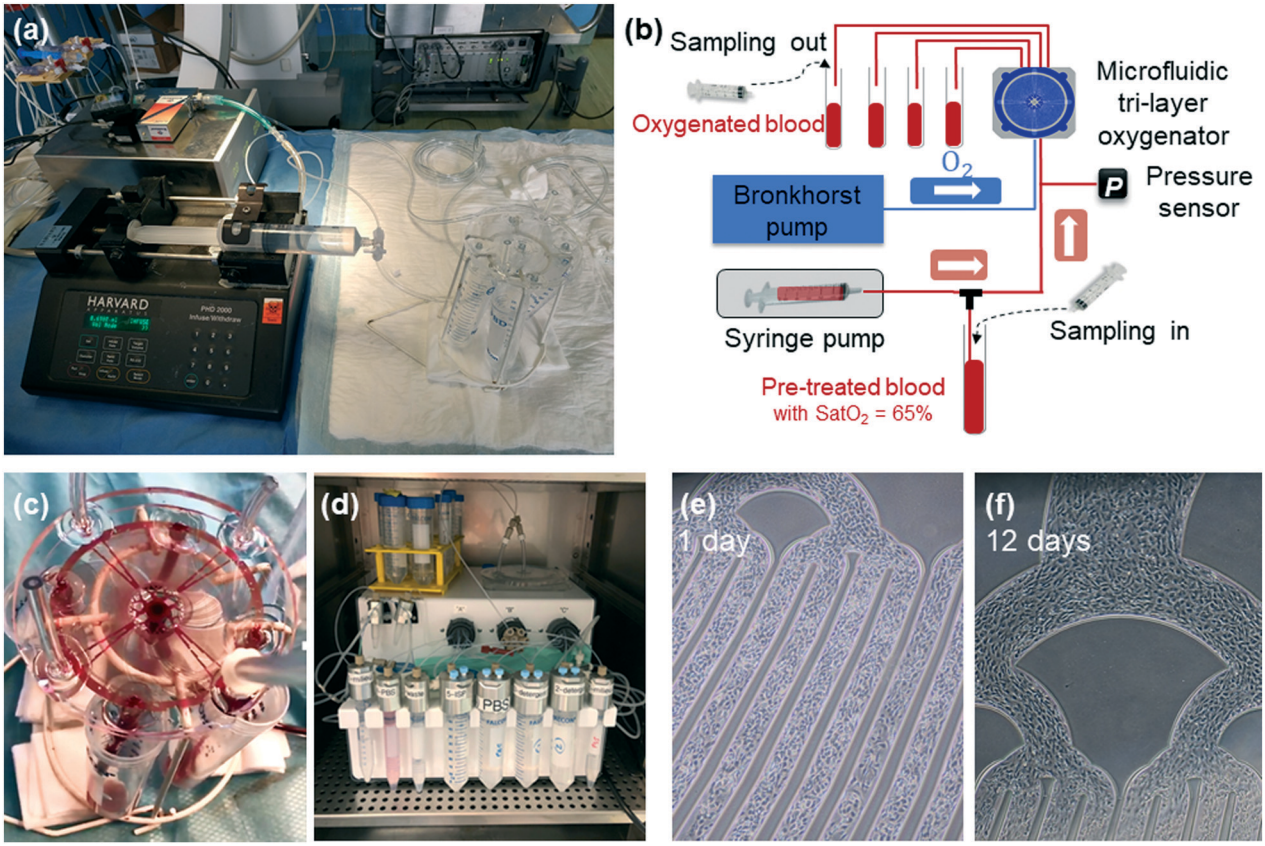

Fig. 3 (a) An image of the whole set-up installed in an operating room at the hospital and (b) the corresponding scheme describing each element. (c) An image of the single trilayer unit oxygenator recorded during the oxygenation/decarbonation experiment. (d) An image of the microfluidic flow control system (MFCS™, Fluigent) installed inside the incubator during the experiment for endothelialization. Optical images recorded during endothelialization in the branching injection parts of one single-layer device at different times after (e) one day and (f) 12 days.

wells as previously described.[28] Endothelial colony-forming cells (ECFCs) appeared after 7–20 days of culture. From passage 1 (P1), cells were seeded at 5000 cells per cm^2 and grew in EGM-2MV medium (Endothelial SingleQuots™ Kit from Lonza). ECFCs at P5 were used to endothelialize the device.

Experiments under flow were performed using a microfluidic flow control system (MFCS™, Fluigent). Fig. 3d shows an image of the whole system connected to one 4 inch single-layer oxygenator inside the incubator. Before seeding the cells, the device was coated for 1 hour at 37 °C with 1 mg ml^{-1} human albumin (Sigma) and 1 U ml^{-1} heparin (Panpharma). Then, after a washing step with PBS 1×, 4×10^6 ECFCs were prepared in 200 µl of PBS 1× and infused into the 4 inch trilayer device. Once the cells adhered, a flow rate of EGM2 (endothelial growth medium 2) of 10 µl min^{-1} was applied during the whole experiment. EGM2 contains 5% FBS and several growth factors, such as rhEGF, VEGF, IGF, and ehFGF, and different additives, such as ascorbic acid, gentamicin, and hydrocortisone, which are necessary for endothelial growth and activity. Devices were incubated at 37 °C and 5% CO_2. Images at different locations of the whole 4 inch surface were taken every day under flow without stopping the fluidic experiment.

3. Results and discussion

3.1 Endothelialization of one 4 inch single trilayer device

This study with endothelial cells is used to validate our new design of blood capillaries including the central branching injector and check the durability of this physiological surface over time. CB ECFCs were used to endothelialize the single-layer device. ECFCs are rare, highly proliferative endothelial cells that are found in bone marrow, the bloodstream and cord blood. ECFCs are highly angiogenic and can migrate to sites of blood vessel injury and contribute to the repair of the damaged vascular structure. We used cord blood ECFCs because these cells display higher performance and immunoregulatory function than adult cells, and they can be easily obtained.[29,30]

To introduce and seed endothelial cells into the device, cells were maintained under a 1 µl min^{-1} flow rate for 60 minutes before the flow rate was increased to 10 µl min^{-1}. To assess endothelialization success and maintenance, images were acquired at different time points from day 1 to day 12 (Fig. 3e and f). Under these fluidic conditions, we were able to successfully endothelialize the single trilayer device for the whole duration of the experiment. Cells started to cover the surface layer of the device starting at day 1 and reached

Open Access Article. Published on 26 July 2021. Downloaded on 1/30/2026 5:49:22 PM.
This article is licensed under a Creative Commons Attribution 3.0 Unported Licence.

confluency on the same day due to the high initial seeding density. No significant detachment of endothelial cells was observed either at the angles or in the straight sections of the channels (Fig. 3e and f). To characterize the endothelial cells, CD31 (an endothelial marker) and cell nuclei (DAPI, as an estimation of cell density) were measured in live flowing cells. We observed homogeneous distribution of the CD31 marker and DAPI, indicating stable full coating in the two week period at the indicated flow conditions (not shown). The advantage of utilizing the MFCS™-EZ perfusion system is to generate a constant pressure-driven flow that provides reliable and highly reproducible conditions. After 13 days under flow, endothelial cells were trypsinized and further analyzed by flow cytometry. The expression of endothelial essential markers such as CD34, CD31, CD144 and VEGFR2 (KDR) assessed before and after flow was similar. These findings indicate that the endothelialization procedure and fluidic conditions at low flow rate (10 μl min^{-1}) do not impact the endothelial markers.

The pioneering work of Borenstein's group had already demonstrated that human umbilical vein endothelial cells (HUVECs) inside blood microchannels were not activated during the experiment.[19] More recently, Hellmann's work[20] has demonstrated the ability to maintain dynamic culture of endothelial cells for 21 days under a flow rate of 1.2 ml min^{-1}. We thus planned further experiments to check the durability of this physiological surface under higher flow and over longer times. In addition, it would be particularly interesting to evaluate both oxygen and carbon dioxide exchange efficiencies within our endothelialized device under whole blood flow. An important future direction for our device would be compatibility studies aimed at establishing if there are any adverse interactions such as immunogenic effects between blood and the ECs. However, this preliminary study validates our new planar circular design over a 4 inch surface.

3.2 Gas exchange performance of one single trilayer unit

The gas exchange properties of one single trilayer unit is then studied. During experiments, the blood flow rate was varied in the range of 0.5–15 ml min^{-1} either in pure oxygen or in air. Testing was performed under these two environments since the ability to work under air with sufficient oxygenation would greatly simplify the use of the microfluidic device. The role of the height H of blood capillaries, H = 85 μm and 105 μm, respectively, in both the pressure drop and the gas exchange performance was studied. Similar subsequent analysis was performed on three different devices with the same geometry. In Fig. 4, for each curve, we report the

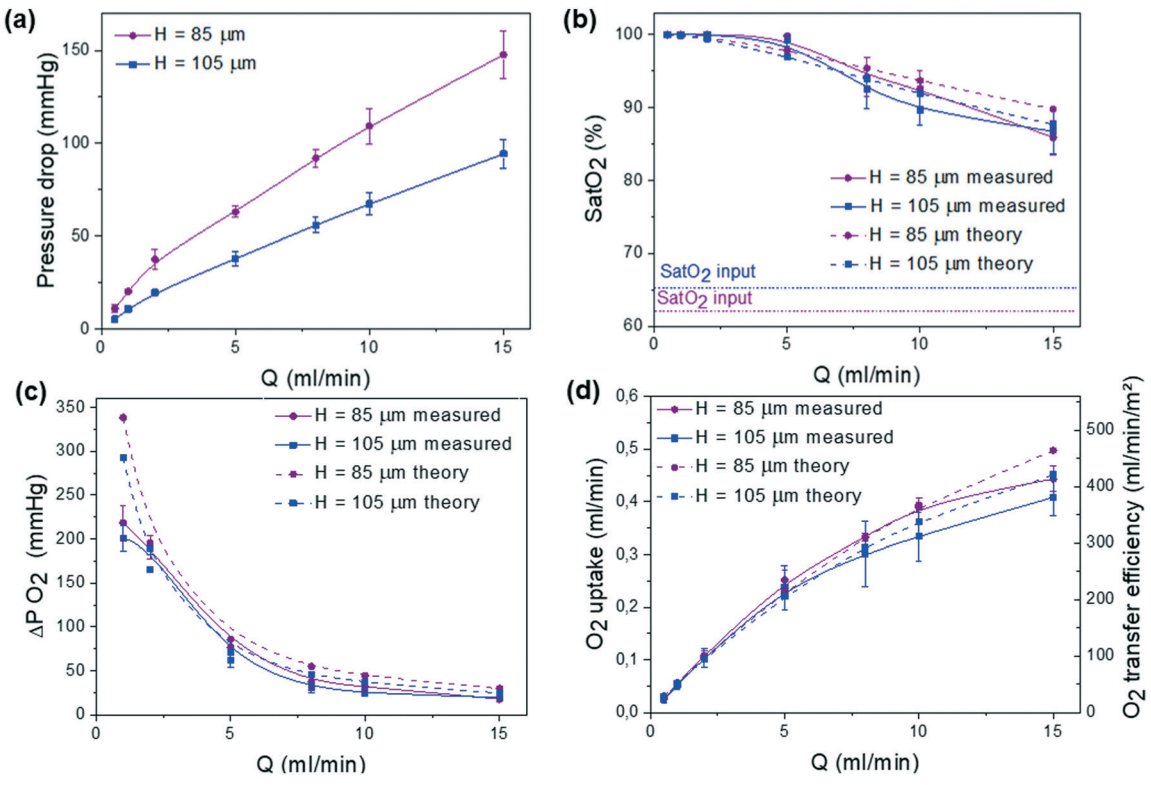

Fig. 4 *In vitro* performances of single-layer devices under pure oxygen with different heights of blood capillaries (H = 85 μm and H = 105 μm): (a) pressure drop at different blood flow rates, (b) variation of the oxygen saturation level Sat(O_2) measured in the blood collected at the output as a function of the blood flow rate (dotted lines give the input values measured before injection into the device), (c) variation of the oxygen partial pressure ΔPO_2 and (d) the corresponding oxygen uptake deduced from Sat(O_2) and ΔPO_2. The theoretical results for the two capillary heights are also represented by dotted lines.

 This journal is © The Royal Society of Chemistry 2021

Open Access Article. Published on 26 July 2021. Downloaded on 1/30/2026 5:49:22 PM.
This article is licensed under a Creative Commons Attribution 3.0 Unported Licence.

average of the 3 corresponding measured values and the error bars give their range.

We have systematically measured the pressure drop ΔP that is related to the blood flow rate Q by $\Delta P = R_h Q$ where R_h is the hydraulic resistance of the microfluidic channel. Fig. 4a shows the evolution of ΔP as a function of Q. Since pressure drop should not exceed 80 mmHg for an arteriovenous connection (normal adult),[31] the optimal H value should be around 105 μm. One should note that this upper bound for pressure drop imposes a maximal working flow rate of around 12 ml min^{-1}.

In an atmospheric environment with pure oxygen, the full saturation of the incoming blood (Sat(O_2) >90%) was achieved at flow rates up to 8 ml min^{-1}, whereas it is shown to slowly decrease at higher flow rates (Fig. 4b). Similarly, the variation of the difference between the outlet and the inlet values of partial pressure that corresponds to the dissolved oxygen in blood $\Delta P(O_2)$ decreases with flow rate due to the shorter residence time, in agreement with theoretical predicted values (Fig. 4c). The mathematical model appears to be more accurate in the flow range of 2–5 ml min^{-1} due to the average values of oxygen solubility S_{B,O_2} and diffusivity D_{B,O_2}. To obtain a better agreement either at small or at large flow, effective S_{B,O_2} and D_{B,O_2} should be calculated on smaller partial pressure ranges. Moreover, the theoretical model[4] does not take into consideration the volume of the gas compartment as oxygen and carbon dioxide partial pressure are assumed to be constant. In a future study, further experiment will be carried out to understand the role of the geometry of the gas compartment (gas channel height) and gas flow rate in gas exchange. Finally, Fig. 4d shows the variation of oxygen uptake as a function of the blood flow rate. In both room air and oxygen environments, the oxygen uptake increased with blood flow rate. The compared gas exchange performance in pure oxygen and air environments is detailed in the ESI† (see Fig. SI.2). As expected, the devices tested under pure oxygen had higher gas exchange efficiencies than the ones tested under air. Also, at high blood flow, devices with thinner channels (H = 85 μm) are able to reach 10% higher oxygen uptake values than devices with thicker channels (H = 105 μm) due to more confined blood volume above the gas-permeable membrane. However, to maintain the pressure drop below 80 mmHg, H = 105 μm was chosen for all subsequent experiments. Note that this value promotes an oxygen transfer efficiency of around 320 ml O_2 per min m^{-2} at the rated flow, similar to the previously reported value for one large single unit by Thompson *et al.*[12]

The second important parameter in the evaluation of any microfluidic oxygenator relates to carbon dioxide release. As shown in Fig. 5, similar to the device with H = 85 μm, the CO_2 release increases with blood flow rate. Theoretical and experimental values are almost similar since solubility and effective diffusivity of CO_2 in the blood do not vary over this range of partial pressures. In addition, to analyze the role of the membrane thickness in gas exchange performance, O_2 uptake and CO_2 release were calculated based on Potkay's model (see the ESI† SI.3A). While the gain in O_2 uptake is only visible at high flow, reducing the thickness of the membrane to around 15 μm can greatly increase CO_2 release even at low blood flow. Moreover, to increase both O_2 uptake and CO_2 release while maintaining the same blood flow rate (up to 15 ml min^{-1}), one would need to enhance the exchange surface area (see predictions in SI.3B†). It appears that the novelty of our system comes from the innovative circular geometry with a very dense network of blood capillaries, producing high oxygen uptake and carbon dioxide release while minimizing priming volume and pressure drop and maintaining low shear in the physiological range.

3.3 The compact integrated stacked system

The proposed design allows stacking multiple 4 inch units in the vertical configuration by simply repeating the fabrication

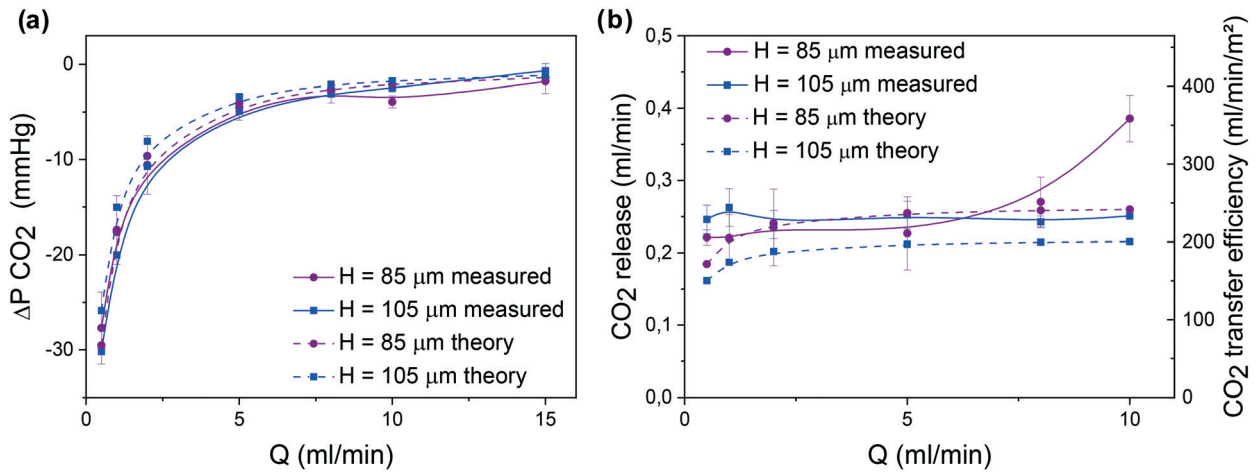

Fig. 5 *In vitro* performance of single-layer devices under pure oxygen with different heights of blood capillaries (H = 85 μm and H = 105 μm): (a) variation of the carbon dioxide partial pressure ΔPCO_2 and (b) the corresponding carbon dioxide release. The theoretical results for the two capillary heights are also represented by dotted lines.

Open Access Article. Published on 26 July 2021. Downloaded on 1/30/2026 5:49:22 PM.
This article is licensed under a Creative Commons Attribution 3.0 Unported Licence.

process of the single unit layer shown in Fig. 2. As illustrated in Fig. 6a, each unit layer can be bonded together with other units with the same blood and air inlet/outlets vertically connected. The extracorporeal circuit including tubes and connectors before and after the device is the same for the stacked layers, which does not increase the priming volume and pressure drop.

We prototyped several devices stacked with 3 or 5 single units to demonstrate the functionality of this vertical stacking. Note that there is no limitation on the number of stacked units. A typical 5 stacked-unit device under blood flow rate is shown in Fig. 6c, with a side view (Fig. 6c1) and top view (Fig. 6c2). In Fig. 6c2, we observe that almost all the blood capillaries are filled with blood. Note that no leaks were detected during the experiments thanks to our wet bonding protocol. More photos are given in SI.4† with two videos included.

Pressure drop and gas exchange performances were studied with pure oxygen at various blood flow rates from 5 to 45 ml min^{-1} (5, 15, 25, 35 and 45 ml min^{-1}) for the 3-stacked units and from 10 to 80 ml min^{-1} (10, 25, 40, 55, 70 and 80 ml min^{-1}) for the 5-stacked units. For 3-stacked units, a similar subsequent analysis was performed on three different devices with the same geometry. In Fig. 6 for each curve, we report the average of the 3 corresponding measured values and the error bars give their range. For the 5-stacked units, only one device was tested.

As shown in Fig. 6b, the variation of oxygen saturation at the output of the blood capillaries for the 3 and 5 stacked layer assembly units is superior to that of the single-layer device under the different flow rates. Sat(O_2) never dropped below 90% saturation (except for the 3 stacked units at 45 ml min^{-1}), while blood flow is 3 times and 5 times higher than for a single unit. This can be explained by the reduced flow rate per each layer thanks to the flow distribution from parallel stacking and by the proximity of the blood channels that can be oxygenated by the sandwiched air channels. The reduced flow rate increases the residual time for oxygenation, thus promoting gas exchange. This also prevents any possible bleeding or clot formation due to excessive flow rates within each capillary channel (variation of ΔPO_2 and ΔPCO_2 is shown in SI.5†). Fig. 6d shows that the pressure drop of the 3 and 5 stacked units never exceeds 80 mmHg in this large range of blood flow rates. This is due to the parallel distribution of fluidic resistance of each layer from the principal inlet/outlets.

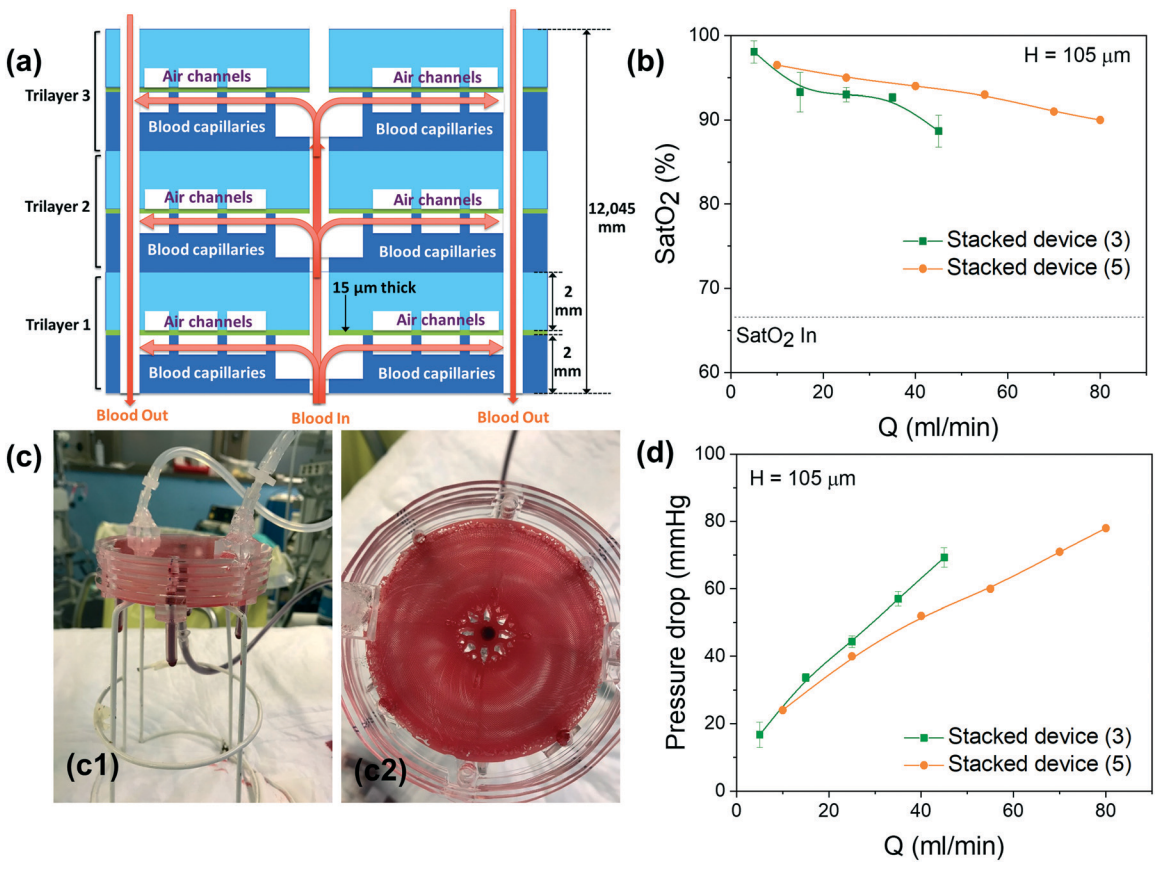

Fig. 6 (a) Cross schematic view of the stacked multilayer device with central blood injection showing the compacity of the whole system and (b) the variation of oxygen saturation level Sat(O_2) at the output as a function of the blood flow rate for 3- and 5-unit stacked devices. (c) An image of one 5-layer device after measurements (cross view (c1) and top view (c2)). (d) The variation of pressure drop as a function of blood flow rate measured for 3- and 5-unit stacked devices.

This journal is © The Royal Society of Chemistry 2021

Open Access Article. Published on 26 July 2021. Downloaded on 1/30/2026 5:49:22 PM.
This article is licensed under a Creative Commons Attribution 3.0 Unported Licence.

As shown in Fig. 7a, the oxygen uptake increases with blood flow rate proportionally to the number of stacked units. Oxygen uptake can therefore be estimated based on the number of stacked layers. However, the CO_2 release shown in Fig. 7b is not proportional to the number of stacked units, which makes it difficult to estimate. This suggests that the influence of the exchange surface exceeds the influence of the blood flow rate. The corresponding oxygen and carbon dioxide transfer efficiencies are presented in Fig. 7c and d. For 3-stacked unit devices at a blood flow rate of 45 ml min^{-1}, the oxygen and carbon dioxide transfer efficiency are about 431 ml O_2 per min m^{-2} and 651 ml CO_2 per min m^{-2}, respectively. For 5-stacked unit devices running at a blood flow rate of 80 ml min^{-1}, the oxygen and carbon dioxide transfer efficiencies are about 490 ml O_2 per min m^{-2} and 902 ml CO_2 per min m^{-2}, respectively. O_2 and CO_2 transfer efficiencies for the stacked devices are always higher than for a single unit. Gas exchange efficiencies as a function of blood flow rate per unit layer for one single unit and 3- and 5-stacked units can be compared in SI.6.† For oxygen, a slight increase in the number of stacked devices is observed. This can be explained by the proximity of the adjacent parallel blood channels that can be oxygenated by the sandwiched gas channels. In addition, compared to the single unit, the flow rate of oxygenation gas can be reduced (maximum 7 ml min^{-1} per unit layer) to lower the pressure drop in the gas channels. For future work, realizing a double-side diffusion by integrating two membranes on each side of the blood network could be a good way to further increase O_2 and CO_2 transfer efficiency per unit layer by doubling the exchange surface area per unit.

Two major challenges for attaining high flow rate microfluidic oxygenators for clinical applications concern the difficulty of maintaining reasonable flow rates within individual capillary channels and the need to have a reasonable pressure drop while increasing the global flow rate by increasing the number of stacked layers. The proposed design of microfluidic oxygenator provides a novel and effective solution that is amenable to further scale-up of blood flow rates. In addition, from the perspective of the manufacturing process, the proposed design allows further scale-up in both the horizontal and the vertical dimensions without major modifications.

The horizontal dimensions can be scaled up by expanding the design to 5-, 6- or even 8-inch wafers which are adapted to the standard microfabrication technologies. For the vertical dimensions, further enhancement of the flow rate is possible by incorporating larger numbers of stacking assembly units, especially through the use of robotic manufacturing technologies.

3.4 Comparison to other microfluidic artificial lungs

Table 1 compares this study to the most recent microfluidic oxygenators to date using oxygen as oxygenation gas.[11,12,18,19]

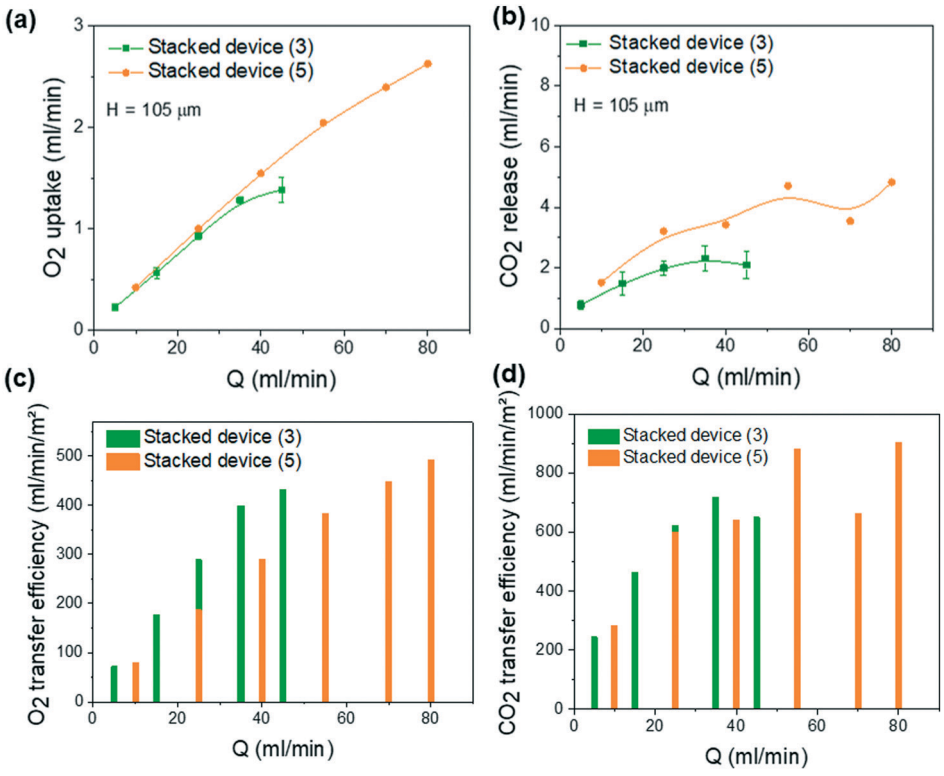

Fig. 7 *In vitro* performance of stacked devices under pure oxygen (with H = 105 μm): (a) variation of the oxygen uptake and (b) of the carbon dioxide release as function of the blood flow rate for 3- and 5-unit stacked devices. The corresponding (c) normalized oxygen and (d) carbon dioxide transfer efficiencies as a function of blood flow rate.

Open Access Article. Published on 26 July 2021. Downloaded on 1/30/2026 5:49:22 PM.
This article is licensed under a Creative Commons Attribution 3.0 Unported Licence.

Table 1 This table compares this current optimized design to previously reported microfluidic oxygenators working with oxygen as oxygenation gas. The reported parameters are the height of the blood capillaries H_c, the membrane thickness e_m, the number of blood unit layers N_{BL}, the pressure drop for a specific blood flow rate Q, the O_2 uptake and CO_2 release for a specific blood flow rate Q, the exchange surface area S_A, the priming volume for only the number of unit layers oxygenator PV_o, the total priming volume with supply tubing PV_t, and the O_2 and CO_2 transfer efficiencies

	H_c (μm)	e_m (μm)	N_{BL}	Pressure drop (mmHg)	O_2 uptake (ml min^{-1})	CO_2 release (ml min^{-1})	S_A (m^2)	PV_o (ml)	PV_t (ml)	O_2 transfer efficiency (ml min^{-1} m^{-2})	CO_2 transfer efficiency (ml min^{-1} m^{-2})	Q (ml min^{-1})
Rieper 2015 (ref. 11)	100	100	10	80	3	3.6	0.12	6.96	—	25	30	50
Gimbel 2016 (ref. 19)	—	30	14	—	1.2	—	0.0046	0.231	—	261	—	25
Thompson 2019 (ref. 12)	30	30	1	66	0.400	—	0.0031	0.47	—	129	—	17
Dabaghi 2019 (ref. 18)	160	30/120	8	95	4.2	4.05	0.0800	8	12.5	52.5	50.63	100
This study, single unit	105	15	1	67	0.34	0.25	0.00107	0.273	1.04	318	235	10
This study, stacked	105	15	3	69	1.38	2.09	0.00321	0.819	2.03	431	651	45

The devices consist of a single or multiple unit layers connected in parallel. At least one of the devices from each major research group studying microfluidic artificial lungs is presented in this table. This was chosen based on the best O_2 uptake with the highest blood flow rate for a pressure drop of less than 100 mmHg (except for Gimbel *et al.*,[19] which does not specify the pressure drop in the device). Note that some studies do not mention the CO_2 release by focusing on O_2 uptake. Since the devices do not have the same gas exchange surface or the same number of unit layers, a comparison of O_2 and CO_2 transfer efficiency is more accurate. As shown in Table 1, the device presented in this study has, by far, the best O_2 and CO_2 transfer efficiencies with values of 431 ml O_2 per min m^{-2} and 651 ml CO_2 per min m^{-2}, respectively. It is therefore the most promising device in terms of oxygenation and decarbonation capacity while offering the most compact structure. With an O_2 uptake and a CO_2 release of ~4.2 ml O_2 per min and ~4.05 ml CO_2 per min, respectively, for a blood flow rate of 100 ml min^{-1}, Dabaghi *et al.* 2019 (ref. 18) have demonstrated the highest O_2 uptake and CO_2 release and the highest blood flow rate for a microfluidic oxygenator to date, thanks to a very large exchange surface of 0.08 m^2 for 8 units connected in parallel. However, in this context, the more compact device proposed here exhibits a lower priming volume thanks to more compact connections. By scaling the device to a blood flow rate of 1 L min^{-1}, 67 layers should be stacked in parallel, and this would correspond to an O_2 transfer rate of 30.82 ml O_2 per min. The CO_2 release cannot be estimated because it is not directly proportional to the number of stacked units (see Fig. 7).

The value of 30.82 ml O_2 per min for the O_2 transfer rate is lower than the minimum O_2 transfer required for a clinical application (45 ml O_2 per min L^{-1} according to AAMI[32]). Based on the numerical simulations presented in the ESI† (SI.3B), an exchange surface area of about 0.003 m^2 on a single unit layer, *i.e.* 3 times larger than the current exchange surface, would allow meeting the clinical requirements. The exchange surface area can be twice as large by realizing a device with a double-sided diffusion, which will increase the O_2 and CO_2 transfer without increasing the pressure drop. The device can also be expanded laterally but in this case the capillaries will be longer, so the pressure drop in the whole system should be reconsidered.

Compared to previously reported devices presented in Table 1, the current 4 inch single-unit design exhibits a very high blood capillary density (see Fig. 1a). Thanks to this compacity, gas exchange may also occur through the lateral sides of the capillary and not only vertically through the membrane. As can be observed in the SEM image (Fig. 2i) showing a cross-view of the trilayer structure, gas exchange is mixed since it occurs laterally through capillary walls (blue arrow) and vertically through the thin membrane (red arrow). It has already been shown that gas exchange occurs with a PDMS thickness of about 100 μm.[11,18] Based on this potential hypothesis, the exchange surface area, calculated as the 2D

This journal is © The Royal Society of Chemistry 2021

Open Access Article. Published on 26 July 2021. Downloaded on 1/30/2026 5:49:22 PM.
This article is licensed under a Creative Commons Attribution 3.0 Unported Licence.

surface of the membrane in contact with blood, is probably underestimated, which would explain the very high measured gas transfer efficiency. To conclude, the compacity of the blood capillary network appears as an important parameter to take into consideration, in addition to all conventional parameters reported in Table 1. In this context, future experiments with devices with different capillary densities should be investigated and compared with 3D numerical simulations.

Conclusions

In this work, a compact and stackable PDMS microfluidic oxygenator was designed for highly efficient gas exchange, and the fabricated devices were tested by oxygenating and decarbonating swine venous blood. The proposed oxygenator is designed at the 4 inch wafer scale to maximize the gas exchange surface area with 256 curved blood microcapillaries and air/oxygen microchannels separated by a 15 μm-thick porous membrane. We took into consideration the fact that such a device would be perfused by the difference in arterial and venous blood pressure. The proposed design allows stacking multiple 4 inch trilayer units to enhance the maximal flow rate without sacrificing the gas exchange efficiency of a single oxygenator unit. We demonstrated the feasibility of vertically stacking 3 or 5 microfluidic oxygenator units, providing a compact size, minimal priming volume, device robustness with high flow rate compatibility and further scalability. The single unit of microfluidic oxygenator, which is fabricated by layer-by-layer assembly based on the "wet-bonding" of PDMS layers, is shown to support high blood flow rates up to 25 ml min^{-1} and to provide high gas exchange efficiency at flow rates up to 15 ml min^{-1}. The 5 unit stacked device allowed oxygenation/decarbonation at blood flow rates up to 80 ml min^{-1}. Furthermore, the biomimetic design of the microfluidic oxygenator allowed long-term sustainable endothelialization of blood micro capillaries, which constitutes an essential step toward enhancing hemocompatibility for clinical applications. Importantly, the proposed design affords low levels of shear stress in the blood compartment as well as low fluidic resistance, which are critical considerations in the design of clinically relevant microfluidic oxygenators. Future work will focus on *in vivo* animal experiments with a larger number of trilayer oxygenator stacking.

Author contributions

J. Lachaux: microfabrication, gas exchange experiments, data curation, analytical analysis, methodology, validation, writing – original draft; G. Hwang: conceptualization, microfabrication, gas exchange experiments, methodology, validation, writing – review and editing; Nassim Arouche and Sina Naserian: cell seeding, endothelialization experiments, validation, writing – review; Abdelmounaim Harouri: microfabrication; Valeria Lotito: gas exchange experiments, analytical analysis; Caterina Casari: gas exchange experiments, coating for cell seeding, review; Thevy Lok: cell seeding, endothelialization experiments; Jean Baptiste Menager, Justin Issard and Julien Guihaire: blood sampling, gas exchange experiments; Cécile V. Denis and Peter J. Lenting: coating for cell seeding, methodology, writing – review; Abdul I. Barakat and Georges Uzan: endothelialization, methodology, validation, writing – review; Olaf Mercier: conceptualization, funding acquisition, methodology, resources, supervision, writing – review; Anne-Marie Haghiri-Gosnet: conceptualization, methodology, gas exchange experiments, data curation, analytical analysis, resources, supervision, writing – review and editing.

Conflicts of interest

There are no conflicts to declare.

Acknowledgements

This work is funded by the French National Research Agency (ANR) as part of the second "investissements d'avenir" program (BioArtlung 2020 Project: ANR-RHUS-0002) coordinated by Professor Olaf Mercier.

Notes and references

1 M. W. Lim, *Anaesthesia*, 2006, **61**, 984.
2 A. Undar, S. Wang and D. A. Palanzo, *Artif. Organs*, 2013, **37**(12), 1080.
3 J. A. Potkay, M. Magnetta, A. Vinson and B. Cmolik, *Lab Chip*, 2011, **11**, 2901.
4 J. A. Potkay, *Biomed. Microdevices*, 2013, **15**(3), 397–406.
5 J. A. Potkay, *Lab Chip*, 2014, **14**, 4122.
6 K. M. Kovach, M. A. LaBarbera, M. C. Moyer, B. L. Cmolik, E. van Lunteren, A. Sen Gupta, J. R. Capadona and J. A. Potkay, *Lab Chip*, 2015, **15**, 1366.
7 T. Kniazeva, J. C. Hsiao, J. L. Charest and J. T. Borenstein, *Biomed. Microdevices*, 2011, **13**, 315.
8 T. Kniazeva, A. A. Epshteyn, J. C. Hsiao, E. S. Kim, V. B. Kolachalama, J. L. Charest and J. T. Borenstein, *Lab Chip*, 2012, **12**, 1686.
9 N. Rochow, W. Wu, E. Chan, D. Nagpal, G. Fusch, P. R. Selvaganapathy, S. Monkman and C. Fusch, *IEEE 25th International Conference on MEMS*, 2012, p. 957.
10 D. M. Hoganson, H. I. Pryor II, E. K. Bassett, I. D. Spool and J. P. Vacanti, *Lab Chip*, 2011, **11**, 700.
11 D. T. Rieper, C. Müller and H. Reinecke, *Biomed. Microdevices*, 2015, **17**, 86.
12 A. J. Thompson, L. J. Ma, T. J. Plegue and J. A. Potkay, *IEEE Trans. Biomed. Eng.*, 2019, **66**(4), 1082.
13 W.-I. Wu, N. Rochow, E. Chan, G. Fusch, A. Manan, D. Nagpal, P. R. Selvaganapathy and C. Fusch, *Lab Chip*, 2013, **13**, 2641.
14 N. Rochow, A. Manan, W. Wu, G. Fusch, S. Monkman, J. Leung, E. Chan, D. Nagpal, D. Predescu, J. Brash, P. R. Selvaganapathy and C. Fusch, *Artif. Organs*, 2014, **38**, 856.

Open Access Article. Published on 26 July 2021. Downloaded on 1/30/2026 5:49:22 PM.
This article is licensed under a Creative Commons Attribution 3.0 Unported Licence.

15 H. Matharoo, M. Dabaghi, N. Rochow, G. Fusch, N. Saraei, M. Tauhiduzzaman, S. Veldhuis, J. Brash, C. Fusch and P. R. Selvaganapathy, *Biomicrofluidics*, 2018, **12**, 014107.
16 M. Dabaghi, G. Fusch, N. Saraei, N. Rochow, J. Brash, C. Fusch and P. R. Selvaganapathy, *Biomicrofluidics*, 2018, **12**, 044101.
17 M. Dabaghi, G. Fusch, N. Saraei, N. Rochow, J. Brash, C. Fusch and P. R. Selvaganapathy, *Lab Chip*, 2018, **18**, 3780.
18 M. Dabaghi, G. Fusch, N. Saraei, N. Rochow, J. Brash, C. Fusch and P. R. Selvaganapathy, *Biomicrofluidics*, 2019, **13**, 034116.
19 A. A. Gimbel, E. Flores, A. Koo, G. Garcia-Cardena and J. T. Borenstein, *Lab Chip*, 2016, **16**, 3227.
20 A. Hellmann, S. Klein, F. Hesselman, S. Djeljadini, T. Schmitz-Rode, S. Jockenhoevel, C. G. Cornelissen and A. L. Thiebes, *Artif. Organs*, 2020, **44**(10), e419–e433.
21 H. R. Williams, R. S. Trask, P. M. Weaver, I. P. Bond and J. R. Soc, *Interface*, 2008, **5**, 55.
22 C. D. Murray, *Proc. Natl. Acad. Sci. U. S. A.*, 1926, **12**, 207.
23 R. W. Barber, K. Cieślicki and D. R. Emerson, in *WIT Transactions on Ecology and the Environment*, 2006, vol. 87, p. 245.
24 J. Barcroft and A. V. Hill, *J. Physiol.*, 1910, **39**(6), 411–428.
25 D. C. Willford and E. P. Hill, *Respir. Physiol.*, 1986, **64**(2), 113–123.
26 A.-M. Haghiri-Gosnet, L. Djeghlaf, J. Lachaux, A. Paris and G. Hwang, Microfluidic gas exchange devices and methods for making same, patent WO2020089116 deposited 25th October 2019 – published 7th May 2020 (PCT EP2019079274).
27 J. B. Lee, K.-H. Choi and K. Yoo, *Micromachines*, 2015, **6**, 1–18.
28 J. B.-D. Ponio, F. El-Ayoubi, F. Glacial, K. Ganeshamoorthy, C. Driancourt, M. Godet, N. Perrière, O. Guillevic, P. O. Couraud and G. Uzan, *PLoS One*, 2014, **9**(1), e84179.
29 S. Naserian, M. E. Abdelgawad, M. Afshar Bakshloo, G. Ha, N. Arouche, J. L. Cohen, B. L. Salomon and G. Uzan, *Cell Commun. Signaling*, 2020, **18**(1), 94.
30 M. Nouri Barkestani, S. Shamdani, M. Afshar Bakshloo, N. Arouche, B. Bambai, G. Uzan and S. Naserian, *Cell Commun. Signaling*, 2021, **19**(1), 1.
31 J. E. Hall, *Guyton and Hall Textbook of Medical Physiology*, PA: Saunders, Philadelphia, 12th edn, 2011.
32 G. J. Myers, *J. Extra-Corpor. Technol.*, 2014, **46**(3), 192–196.

 This journal is © The Royal Society of Chemistry 2021